In Silico Capture of Noble Gas Atoms with a Light Atom Molecule

Stefan Mebs,[1]* Jens Beckmann[2]

[1] *Institut für Experimentalphysik, Freie Universität Berlin, Arnimallee 14, 14195 Berlin, Germany*

[2] *Institut für Anorganische Chemie und Kristallographie, Universität Bremen, Leobener Straße 7, 28359 Bremen, Germany*

Supporting Information

The following two tables, S1 and S2, require explanations about the used color-code. The realization of this project was connected with enormous computational efforts; a rough estimate of the 55 DFT-relaxed structures (each with more than 120 atoms) as well as numerous additional calculations presented here yields about 500.000 h of computational time with state-of-the-art processors (not to mention the roughly same number of structures not presented here). Some of those structures converged fast, others converged almost and stayed in this status for 20-30 optimization cycles without further changing the overall energy in a significant fashion (± 0.5 kJ mol^{-1}). Since all but one ligand systems are not capable to energy efficiently capture Ng atoms, it was decided to stop those cases after two weeks with 20 processors each, which tend to remain in this volatile state. The best performer, $[(5\text{-}Ph_2B\text{-}xan\text{-}4\text{-})_3Si\cdot Ng]^+$, was fully converged. Due to the same reasons, the calculations were conducted at the b3pw91-D3/6-31+G* level of theory, and only for the best performer, additional single-point calculations were done at the b3pw91-D3/6-311+G(2df,p) level of theory using the b3pw91-D3/6-31+G* optimized coordinated. Basis-set superposition errors are known to give wrong (too strong) adduct formation energies. In order to compensate for that, BSSE correction was conducted explicitly using the counterpoise method for the best performer at both levels of theory, and the energetic add-on extracted from those corrections was applied to all other adduct structures as an estimate. The mentioned limitations and methods result in the following color code:

Light green highlighted absolute energies: full convergence achieved

Light orange highlighted absolute energies: almost full convergence achieved

Yellow highlighted absolute energies: Single-point calculations

Blue highlighted absolute energies: BSSE-correction

Green highlighted relative energies: $\Delta E < 0$ – model is favorable

Orange highlighted relative energies: $\Delta E > 0$ – model is unfavorable

Red colored numbers: BSSE add-on applied to all adduct structures

Bold formatted relative energies: Final results as listed in Table 1.

§ Calculations at b3pw91-D3/6-311+G(2df,p)

Table S1. Absolute and relative energies of $[(R_2E\text{-}spacer\text{-})_3Si \cdot Ng]^+$

spacer	E	R	state	E (a.u.)	LS+Ng (a.u.)	ΔE (a.u.)	ΔE (kJ mol⁻¹)	BSSE (kJ mol⁻¹)	ΔE$_{corr}$ (kJ mol⁻¹)
ace	B	C$_6$F$_5$	start	-6116.2702		-0.0132	-34.8		
ace	B	C$_6$F$_5$	dead-end	-6116.2570					
ace	B	C$_6$F$_5$	active	-6115.4058					
ace	B	C$_6$F$_5$	He	-6118.2894	-6118.3075	0.0181	47.6	4.5	52.1
ace	B	Ph	start	-3140.3279		-0.0082	-21.4		
ace	B	Ph	dead-end	-3140.3198					
ace	B	Ph	active	-3139.4832					
ace	B	Ph	He	-3142.3745	-3142.3849	0.0104	27.3	4.5	31.8
ace	Ga	C$_6$F$_5$	start	-11810.6579		0.0320	83.9		
ace	Ga	C$_6$F$_5$	dead-end	-11810.6899					
ace	Ga	C$_6$F$_5$	active	-11809.7906					
ace	Ga	C$_6$F$_5$	He	-11812.6825	-11812.6923	0.0098	25.6	4.5	30.1
bip	B	Ph	start	-3136.4596		-0.0027	-7.1		
bip	B	Ph	dead-end	-3136.4569					
bip	B	Ph	active	-3135.6106					
bip	B	Ph	He	-3138.5090	-3138.5123	0.0033	8.7	4.5	13.2
bip	Ga	C$_6$F$_5$	start	-11806.7610		0.0202	53.2		
bip	Ga	C$_6$F$_5$	dead-end	-11806.7813					
bip	Ga	C$_6$F$_5$	active	-11805.8919					
bip	Ga	C$_6$F$_5$	He	-11808.7857	-11808.7936	0.0079	20.7	4.5	25.2
bip	Ga	Ph	start	-8830.7569		0.0129	33.9		
bip	Ga	Ph	dead-end	-8830.7698					
bip	Ga	Ph	active	-8829.8994					
bip	Ga	Ph	He	-8832.8003	-8832.8011	0.0008	2.0	4.5	6.5
txn	B	C$_6$F$_5$	start	-7425.0050		-0.0027	-7.0		
txn	B	C$_6$F$_5$	dead-end	-7425.0024					
txn	B	C$_6$F$_5$	active	-7424.1460					
txn	B	C$_6$F$_5$	He	-7427.0455	-7427.0477	0.0022	5.9	4.5	10.4
txn	B	C$_6$F$_5$	Kr	-10175.2407	-10175.2233	-0.0174	-45.7	60.2	14.5
txn	Ga	C$_6$F$_5$	start	-13119.3540		-0.0015	-3.9		
txn	Ga	C$_6$F$_5$	dead-end	-13119.3525					
txn	Ga	C$_6$F$_5$	active	-13118.5259					
txn	Ga	C$_6$F$_5$	He	-13121.4206	-13121.4276	0.0070	18.3	4.5	22.8
txn	Ga	C$_6$F$_5$	Kr	-15869.6003	-15869.6032	0.0029	7.6	60.2	67.8

Light green: fully converged. Light orange: almost converged.

Green: ΔE < 0. Orange: ΔE > 0.

Table S2. Absolute and relative energies of [(5-Ph$_2$B-xan-4-)$_3$Si·Ng]$^+$ (**2d-g**)

L	E	R	state	E (a.u.)	LS+Ng (a.u.)	ΔE (a.u.)	ΔE (kJ/mol)	BSSE (kJ/mol)	ΔE$_{corr}$ (kJ/mol)
xan	B	C6F5	start	-6456.1364		-0.0127	**-33.4**		
xan	B	C6F5	dead-end	-6456.1237					
xan	B	C6F5	active	-6455.2877					
xan	B	C6F5	He	-6458.1712	-6458.1894	0.0182	**47.7**	4.5	**52.2**
xan	B	C6F5	Ne	-6584.1459	-6584.1622	0.0163	**42.9**	5.7	**48.6**
xan	B	C6F5	Ar	-6982.7432	-6982.7520	0.0087	**22.9**	4.2	**27.1**
xan	B	C6F5	Kr	-9206.3872	-9206.3649	-0.0223	**-58.6**	60.2	**1.6**
xan	Ga	C6F5	start	-12150.4941		-0.0059	**-15.4**		
xan	Ga	C6F5	dead-end	-12150.4882					
xan	Ga	C6F5	active	-12149.6620					
xan	Ga	C6F5	He	-12152.5253	-12152.5637	0.0384	**100.8**	4.5	**105.3**
xan	Ga	C6F5	Ne	-12278.4960	-12278.5365	0.0405	**106.4**	5.7	**112.1**
xan	Ga	C6F5	Ar	-12677.0937	-12677.1263	0.0325	**85.4**	4.2	**89.6**
xan	Ga	C6F5	Kr	-14900.7359	-14900.7392	0.0033	**8.7**	60.2	**68.9**
xan	B	Ph	start	-3480.1911		-0.0143	**-37.5**		
xan	B	Ph	dead-end	-3480.1768				BSSE add-on (kJ mol^{-1})	incl. BSSE (kJ mol^{-1})
xan	B	Ph	active	**-3479.3411**					
xan	B	Ph	He	-3482.2447	-3482.2428	-0.0019	**-4.9**	4.5	**-0.4**
xan	B	Ph	Ne	-3608.2199	-3608.2157	-0.0042	**-11.0**	5.7	**-5.3**
xan	B	Ph	Ar	-4006.8188	-4006.8054	-0.0134	**-35.3**	4.2	**-31.1**
xan	B	Ph	Kr	-6230.4618	-6230.4184	-0.0434	**-113.9**	60.2	**-53.7**
xan§	B	Ph	start	-3481.0317		-0.0142	**-37.3**		
xan§	B	Ph	dead-end	-3481.0175					
xan§	B	Ph	active	-3480.1808					
xan§	B	Ph	He	-3483.0888	-3483.0880	-0.0008	**-2.2**	1.6	**-0.6**
xan§	B	Ph	Ne	-3609.1036	-3609.0988	-0.0049	**-12.8**	7.6	**-5.2**
xan§	B	Ph	Ar	-4007.6928	-4007.6784	-0.0144	**-37.8**	2.9	**-34.9**
xan§	B	Ph	Kr	-6233.9428	-6233.9185	-0.0244	**-64.0**	5.9	**-58.1**

L	E	R	state	"Ng"	"LS"	"Ng" + "LS"	adduct	ΔE (a.u.)	ΔE (kJ/mol)
xan	B	Ph	He	-2.9034	-3479.3413	-3482.2446	-3482.2447	0.0000	**-0.1**
xan	B	Ph	Ne	-128.8764	-3479.3416	-3608.2179	-3608.2199	-0.0019	**-5.1**
xan	B	Ph	Ar	-527.4653	-3479.3416	-4006.8069	-4006.8188	-0.0119	**-31.4**
xan	B	Ph	Kr	-2751.0992	-3479.3409	-6230.4401	-6230.4618	-0.0217	**-56.9**
xan§	B	Ph	He	-2.9077	-3480.1809	-3483.0886	-3483.0888	-0.0002	**-0.6**
xan§	B	Ph	Ne	-128.9206	-3480.1810	-3609.1017	-3609.1036	-0.0020	**-5.2**
xan§	B	Ph	Ar	-527.4983	-3480.1811	-4007.6794	-4007.6928	-0.0134	**-35.2**
xan§	B	Ph	Kr	-2753.7394	-3480.1802	-6233.9196	-6233.9428	-0.0233	**-61.1**
				Ng(gas)	Ng(gas)§		LS-opt-Ng		
			He	-2.9017	-2.9072		-3479.3412	-0.0001	-0.3
			Ne	-128.8745	-128.9180		-3479.3412	-0.0001	-0.2
			Ar	-527.4643	-527.4976		-3479.3410	0.0001	0.3
			Kr	-2751.0772	-2753.7376		-3479.3399	0.0012	3.2

Yellow: single-point calculations. Blue: BSSE calculations. § 6-311+G(2df,p) basis set.

Table S3. Thermodynamic properties of [(5-Ph$_2$B-*xan*-4-)$_3$Si·Ng]$^+$ (**2d-g**)

model	empty active	small (a.u.)				small + empty (a.u.)			
		He	Ne	Ar	Kr	He	Ne	Ar	Kr
E	-3479.341	-2.902	-128.875	-527.464	-2751.077	-3482.243	-3608.216	-4006.805	-6230.418
ZPE-corr (H/n)	1.086	0.000	0.000	0.000	0.000	1.086	1.086	1.086	1.086
TD-E corr	1.152	0.001	0.001	0.001	0.001	1.153	1.153	1.153	1.153
TD-H corr	1.153	0.002	0.002	0.002	0.002	1.155	1.155	1.155	1.155
TD-G corr	0.983	-0.012	-0.014	-0.015	-0.016	0.971	0.969	0.968	0.967
E+ZPE	-3478.255	-2.902	-128.875	-527.464	-2751.077	-3481.156	-3607.129	-4005.719	-6229.332
E+TD-E	-3478.189	-2.900	-128.873	-527.463	-2751.076	-3481.090	-3607.063	-4005.652	-6229.265
E+TD-H	-3478.188	-2.899	-128.872	-527.462	-2751.075	-3481.088	-3607.061	-4005.650	-6229.263
E+TD-G	-3478.358	-2.914	-128.889	-527.479	-2751.093	-3481.271	-3607.247	-4005.837	-6229.451
E-TD (Kcal/mol)	722.665	0.889	0.889	0.889	0.889	723.554	723.554	723.554	723.554
CV (Cal/molK)	263.422	2.981	2.981	2.981	2.981	266.403	266.403	266.403	266.403
S (Cal/molK)	356.557	30.125	34.919	36.984	39.195	386.682	391.476	393.541	395.752

model	adduct (a.u.)				adduct - small+empty (a.u.)			
	He	Ne	Ar	Kr	He	Ne	Ar	Kr
E	-3482.245	-3608.220	-4006.819	-6230.462	-0.002	-0.004	-0.013	-0.043
ZPE-corr (H/n)	1.087	1.087	1.088	1.087	0.001	0.000	0.001	0.001
TD-E corr	1.155	1.154	1.155	1.155	0.002	0.001	0.002	0.002
TD-H corr	1.156	1.155	1.156	1.156	0.001	0.000	0.001	0.001
TD-G corr	0.981	0.977	0.983	0.982	0.010	0.008	0.015	0.015
E+ZPE	-3481.158	-3607.133	-4005.731	-6229.374	-0.001	-0.004	-0.012	-0.042
E+TD-E	-3481.090	-3607.065	-4005.664	-6229.307	0.000	-0.003	-0.012	-0.041
E+TD-H	-3481.089	-3607.064	-4005.663	-6229.306	-0.001	-0.004	-0.013	-0.042
E+TD-G	-3481.264	-3607.243	-4005.836	-6229.479	0.008	0.004	0.001	-0.028
E-TD (Kcal/mol)	724.633	724.449	724.727	724.705	1.079	0.895	1.173	1.151
CV (Cal/molK)	269.129	269.352	269.022	269.136	2.726	2.949	2.619	2.733
S (Cal/molK)	367.895	375.418	364.093	365.715	-18.787	-16.058	-29.448	-30.037

model	adduct - small+empty (kJ mol^{-1})				BSSE-corrected (kJ mol^{-1})			
	He	Ne	Ar	Kr	He	Ne	Ar	Kr
E	-4.9	-11.0	-35.3	-113.9	-0.4	-5.3	-31.1	-53.7
					4.5	**5.7**	**4.2**	**60.2**
ZPE-corr (H/n)	2.4	0.9	3.2	2.9				
TD-E corr	4.5	3.7	4.9	4.8				
TD-H corr	2.0	1.3	2.4	2.3				
TD-G corr	25.5	21.3	39.2	39.8				
E+ZPE	-3.1	-9.9	-32.6	-110.6	1.4	-4.2	-28.4	-50.4
E+TD-E	-1.0	-7.0	-31.0	-108.6	3.5	-1.3	-26.8	-48.4
E+TD-H	-3.5	-9.5	-33.4	-111.1	1.0	-3.8	-29.2	-50.9
E+TD-G	20.0	10.5	3.3	-73.6	24.5	16.2	7.5	-13.4
E-TD (Kcal/-mol)	0.26	0.21	0.28	0.28				
CV (Cal/molK)	0.65	0.70	0.63	0.65				
S (Cal/molK)	-4.49	-3.84	-7.04	-7.18				

BSSE correction given as bold red numbers; BSSE corrected Gibbs free energies highlighted in yellow.

Table S4. Grimme-D3 dispersion energy parts for $[(5-Ph_2B-xan-4-)_3Si\cdot(Ng)]^{(+)}(H)$

model	E(disp) a.u.	E(disp) kJ mol^{-1}	ΔE(disp) kJ mol^{-1}
neutral	-0.4890	-1283.8	
dead-end	-0.4819	-1265.1	
active	-0.4842	-1271.4	
no_He	-0.4834	-1269.2	
no_Ne	-0.4836	-1269.7	
no_Ar	-0.4834	-1269.2	
no_Kr	-0.4865	-1277.2	
average		**-1270.5**	
He	-0.4863	-1276.8	-6.3
Ne	-0.4895	-1285.1	-14.6
Ar	-0.5037	-1322.5	-52.0
Kr	-0.5160	-1354.8	-84.3
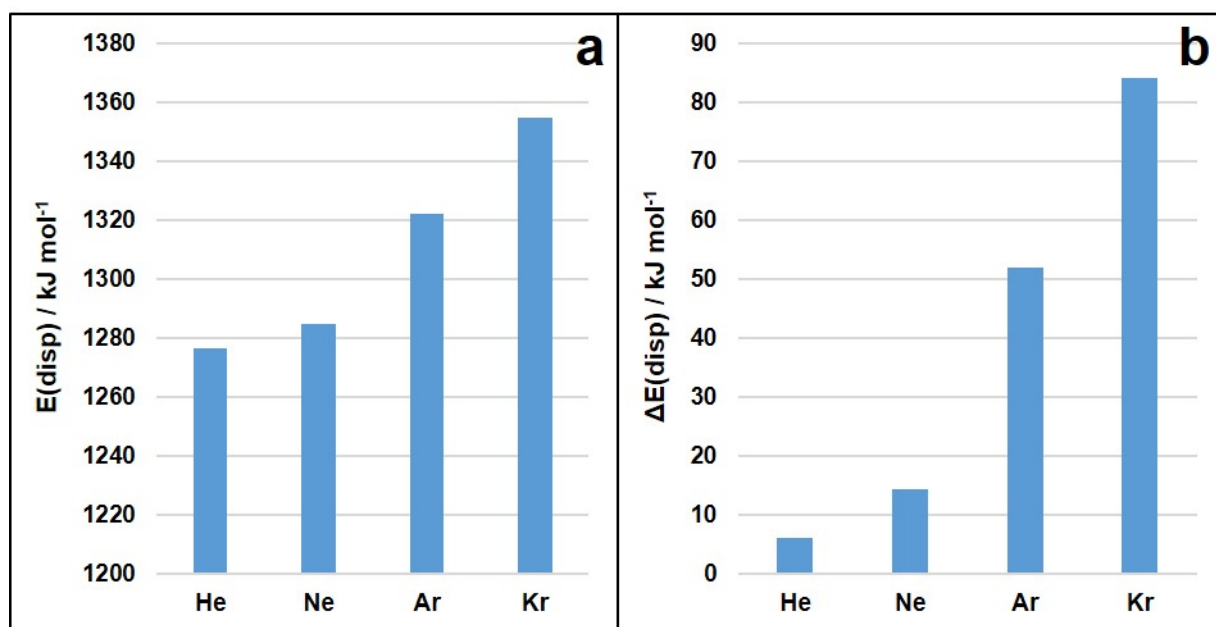
Figure S1. Grimme-D3 dispersion energy parts for $[(5-Ph_2B-xan-4-)_3Si\cdot(Ng)]^{(+)}(H)$: (a) absolute values, (b) the averaged value of all calculations including only the active ligand systems (active state and "no Ng states") was subtracted from the respective models including Ng atoms to quantify the relevance of dispersion between ligand system and Ng atoms, see Table S4. Signs are inverted for display purposes.

Table S5. Estimation of the energy requirements for the hydride abstraction step[§]

model	start (2a)	active (2c)	$^{(+)}CPh_3$	CPh_3H	$2a + {}^{(+)}CPh_3$	$2c + CPh_3H$	diff. (a.u.)	diff. (kJ/mol)
E	-3480.2067	-3479.3940	-732.6887	-733.4911	-4212.8955	-4212.8852	0.0103	27.0
ZPE-corr (H/n)	1.0937	1.0878	0.2818	0.2919	1.3756	1.3797	0.0041	10.7
TD-E corr	1.1581	1.1523	0.2963	0.3069	1.4544	1.4592	0.0048	12.5
TD-H corr	1.1590	1.1532	0.2973	0.3079	1.4563	1.4611	0.0048	12.5
TD-G corr	0.9945	0.9882	0.2396	0.2468	1.2341	1.2349	0.0008	2.2
E+ZPE	-3479.1130	-3478.3063	-732.4069	-733.1992	-4211.5199	-4211.5055	0.0144	37.8
E+TD-E	-3479.0487	-3478.2418	-732.3924	-733.1842	-4211.4411	-4211.4260	0.0151	39.5
E+TD-H	-3479.0477	-3478.2408	-732.3915	-733.1833	-4211.4392	-4211.4241	0.0151	39.5
E+TD-G	-3479.2123	-3478.4059	-732.4491	-733.2444	-4211.6614	-4211.6502	0.0111	29.2
E-TD (Kcal/mol)	726.7000	723.0560	185.9580	192.5900	912.6580	915.6460	2.9880	12.5
CV (Cal/molK)	263.0360	262.7270	59.0850	60.0450	322.1210	322.7720	0.6510	2.7
S (Cal/molK)	346.3110	347.3480	121.3310	128.5660	467.6420	475.9140	8.2720	34.6

[§] b3pw91-D3/6-31+G* level of theory including dispersion *and* solvation (CH_2Cl_2)

Table S6. Relevant bond distances (in Å) of $[(5\text{-Ph}_2\text{B-}xan\text{-}4\text{-})_3\text{Si·Ng}]^+$ (**2d-g**)

Si	$r_{C(Ng)}$	$r_{C(Si)}$	Σr_C	$r_{V(Ng)}$	$r_{V(Si)}$	Σr_V	$\Delta r(Si)$		$d(Ng\text{-}Si)$	%(C,V)
He	0.46	1.16	1.62	1.43	2.19	3.62	2.00		**3.149**	76.5
Ne	0.67	1.16	1.83	1.58	2.19	3.77	1.94		**3.119**	66.4
Ar	0.96	1.16	2.12	1.83	2.19	4.02	1.90		**2.890**	40.5
Kr	1.17	1.16	2.33	2.25	2.19	4.44	2.11		**2.707**	17.9

B	$r_{C(Ng)}$	$r_{C(B)}$	Σr_C	$r_{V(Ng)}$	$r_{V(B)}$	Σr_V	$\Delta r(B)$		$d(Ng\text{-}B)$	%(C,V)
He	0.46	0.85	1.31	1.43	1.91	3.34	2.03		**3.323**	99.2
Ne	0.67	0.85	1.52	1.58	1.91	3.49	1.97		**3.332**	92.0
Ar	0.96	0.85	1.81	1.83	1.91	3.74	1.93		**3.384**	81.5
Kr	1.17	0.85	2.02	2.25	1.91	4.16	2.14		**3.379**	63.5

O	$r_{C(Ng)}$	$r_{C(O)}$	Σr_C	$r_{V(Ng)}$	$r_{V(O)}$	Σr_V	$\Delta r(O)$		$d(Ng\text{-}O)$	%(C,V)
He	0.46	0.63	1.09	1.43	1.50	2.93	1.84		**3.543**	133.3
Ne	0.67	0.63	1.30	1.58	1.50	3.08	1.78		**3.535**	125.6
Ar	0.96	0.63	1.59	1.83	1.50	3.33	1.74		**3.428**	105.7
Kr	1.17	0.63	1.80	2.25	1.50	3.75	1.95		**3.340**	79.0

d(E,B)	Si-B1	Si-B1	Si-B1	B1-B2	B1-B3	B2-B3	Ø(Si-B)	Ø(B-B)	Δ(Si-B)	Δ(B-B)
act	4.883	4.882	4.883	5.659	5.664	5.660	4.883	5.661		
He	4.893	4.891	4.895	5.694	5.699	5.697	4.893	5.697	0.01	0.04
Ne	4.892	4.891	4.895	5.706	5.705	5.706	4.893	5.705	0.01	0.04
Ar	4.877	4.876	4.877	5.742	5.736	5.738	4.877	5.739	-0.01	0.08
Kr	4.819	4.820	4.818	5.674	5.674	5.675	4.819	5.674	-0.06	0.01

r_C or r_V is the molecular single bond covalent or van der Waals radius as listed in the webelements page (https://www.webelements.com/), Δr is the difference between covalent and van der Waals radius. d(Ng-Si/B/O) is the DFT distance after structural relaxation (in bold, b3pw91-D3/6-31+G* level of theory). %(C,V) is the relative position of the DFT atom-atom distance within the range spanned by the difference between sum of covalent radii and van der Waals radii, i.e. a %(C,V) value larger than 100% indicates no interaction, a %(C,V) value between 50-100% a rather weak electrostatic interaction, and a %(C,V) value below 50% a polarized interaction with non-negligible covalent bond contributions.
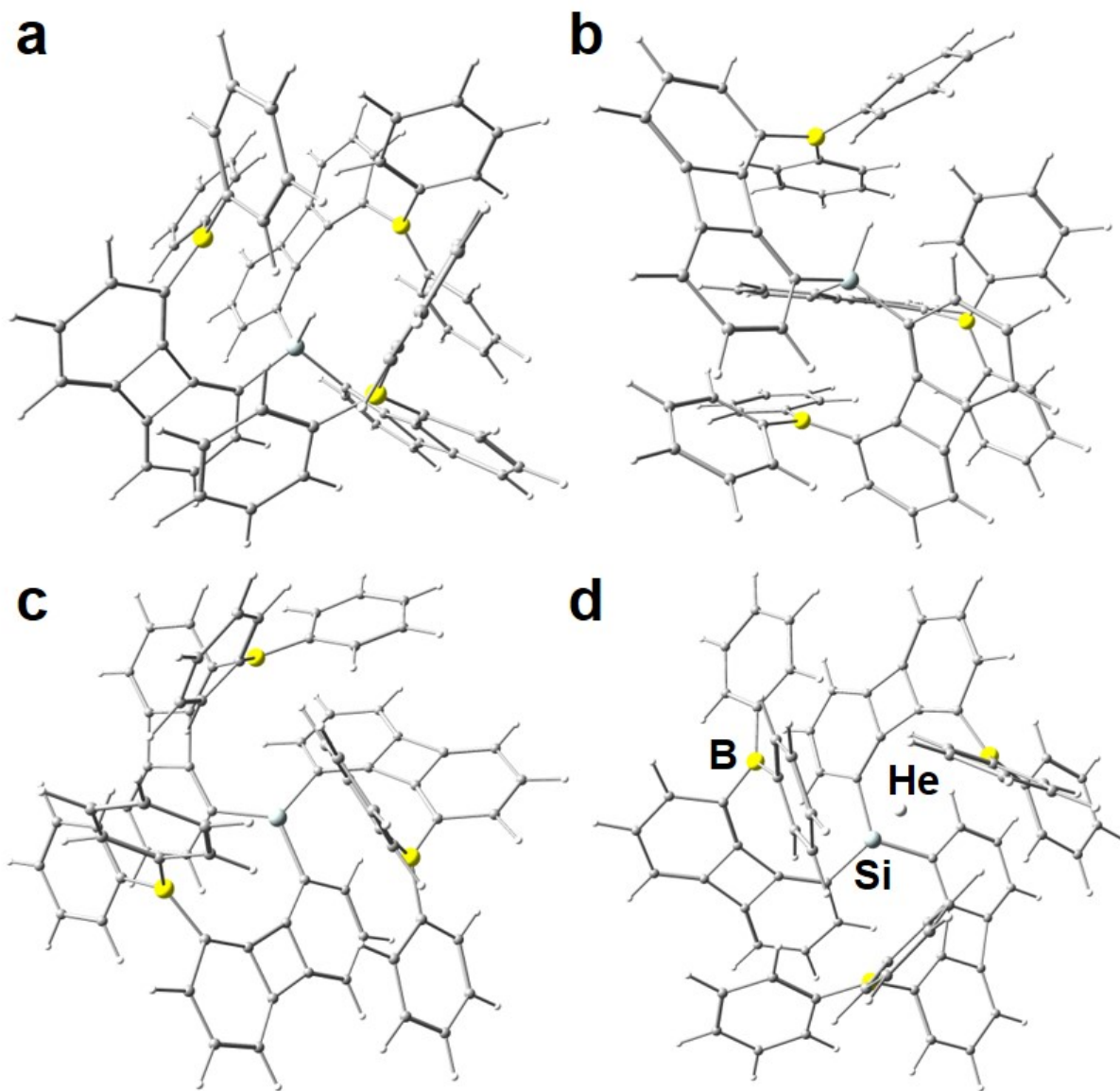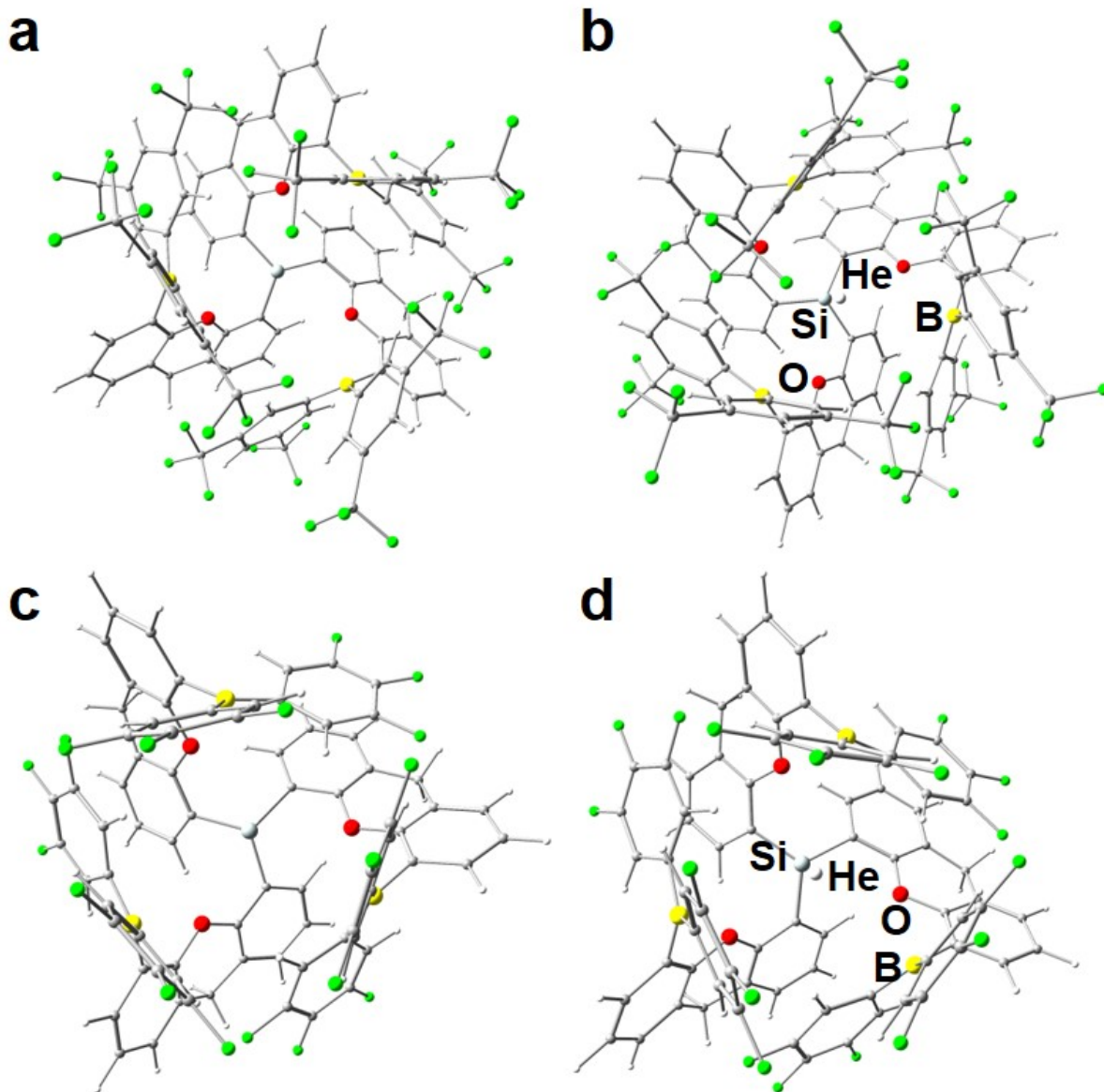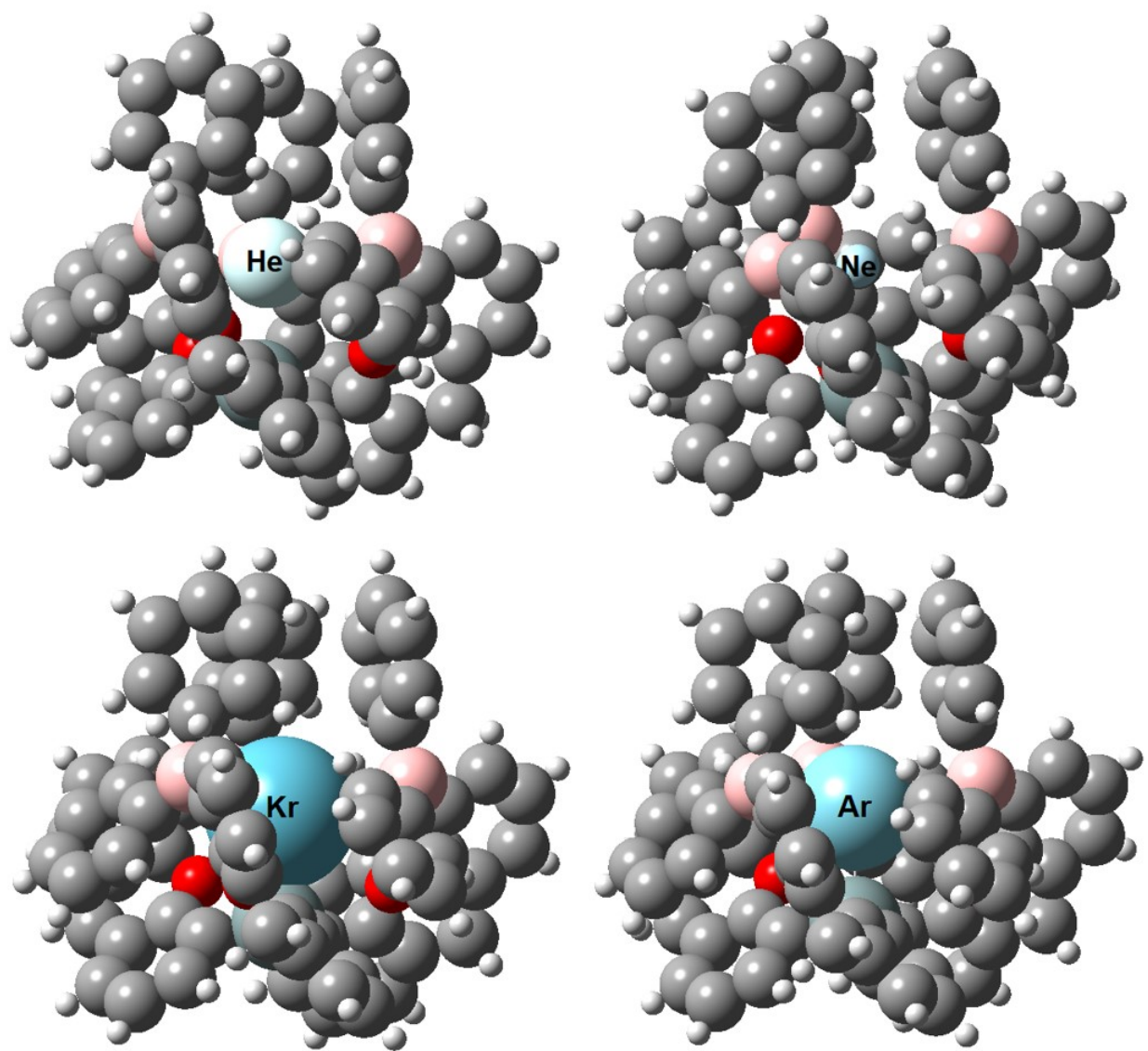
Figure S2. Relaxed gas-phase geometries of (a) the neutral starting state [(5-Ph$_2$B-*bip*-4-)$_3$Si]H in the preferred orientation, (b) Neutral starting state [(5-Ph$_2$B-*bip*-4-)$_3$Si]H in the unfavorable orientation, (c) Active state [(5-Ph$_2$B-*bip*-4-)$_3$Si]$^+$, (d) He-adduct. [(5-Ph$_2$B- *bip*-4-)$_3$Si·He]$^+$.
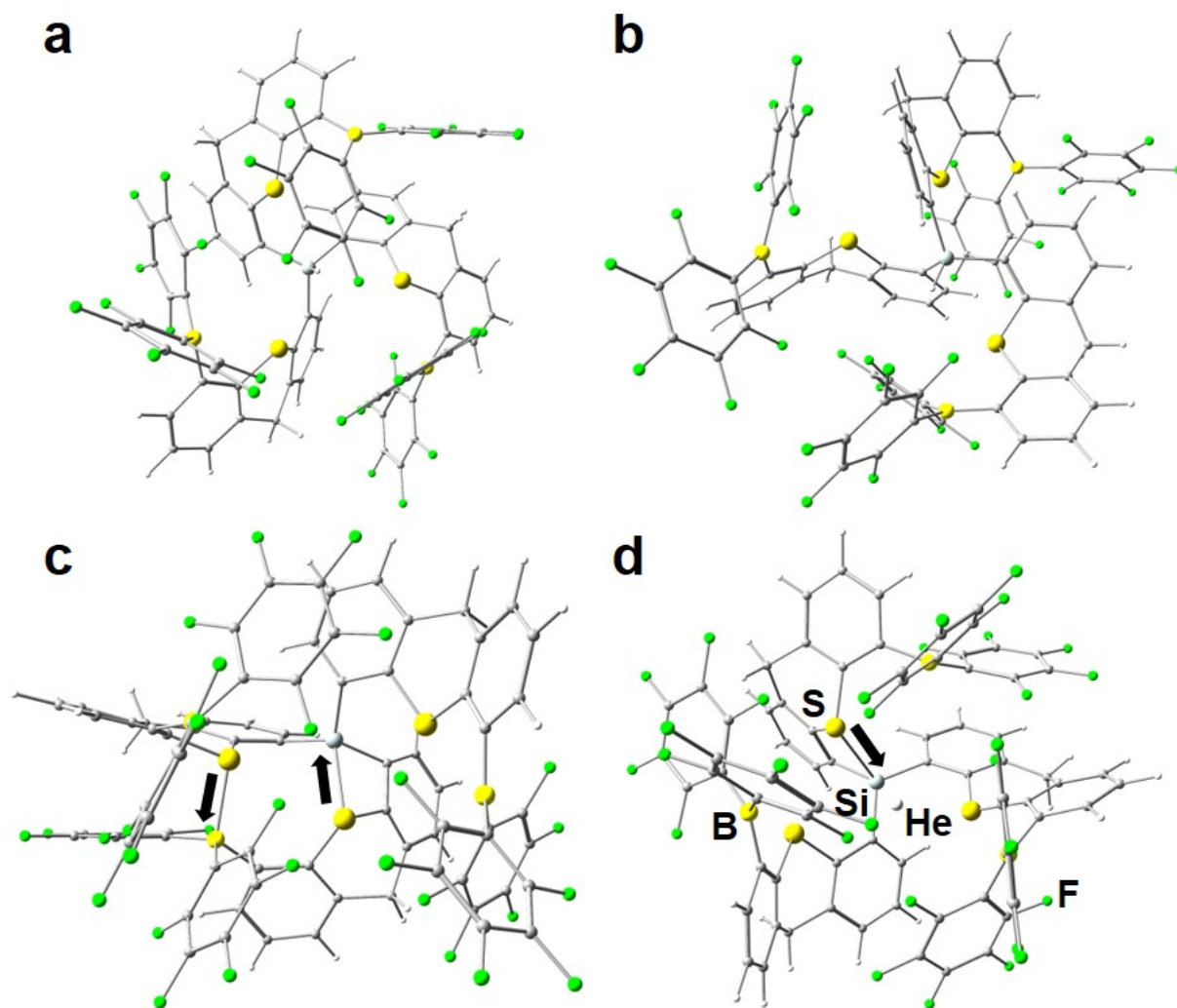
Figure S3. Relaxed gas-phase geometries of (a) the neutral starting state [(5-Ph$_2$B-*txn*-4-)$_3$Si]H in the preferred orientation, (b) Neutral starting state [(5-Ph$_2$B-*txn*-4-)$_3$Si]H in the unfavorable orientation, (c) Active state [(5-Ph$_2$B-*txn*-4-)$_3$Si]$^+$, which is quenched by a short S···Si (d(S,Si) = 2.360 Å) and a short S···B (d(S,B) = 2.162 Å) interaction, (d) He-adduct [(5-Ph$_2$B-*txn*-4-)$_3$Si·He]$^+$ Unfavorable Lewis acid Lewis base contacts are highlighted by black arrows.

Figure S4. Relaxed gas-phase geometries of $[(5\text{-}R_2B\text{-}xan\text{-}4\text{-})_3Si]^+$ variants. (a) R = C_6H_3(m-$CF_3)_2$; active state in the preferred orientation, (b) Corresponding $[(5\text{-}R_2B\text{-}xan\text{-}4\text{-})_3Si·He]^+$ He adduct, (c) R = $C_6H_2F_3$; active state in the preferred orientation, (d) Corresponding He adduct.

Figure S5. Van der Waals representation of the [(5-Ph$_2$B-*xan*-4-)$_3$Si·Ng]$^+$ adducts (**2d-g**). VdW-radii used as implemented in GaussView3. Color code: Si (light gray), O (red), B (yellow), Ng (light to deep blue).
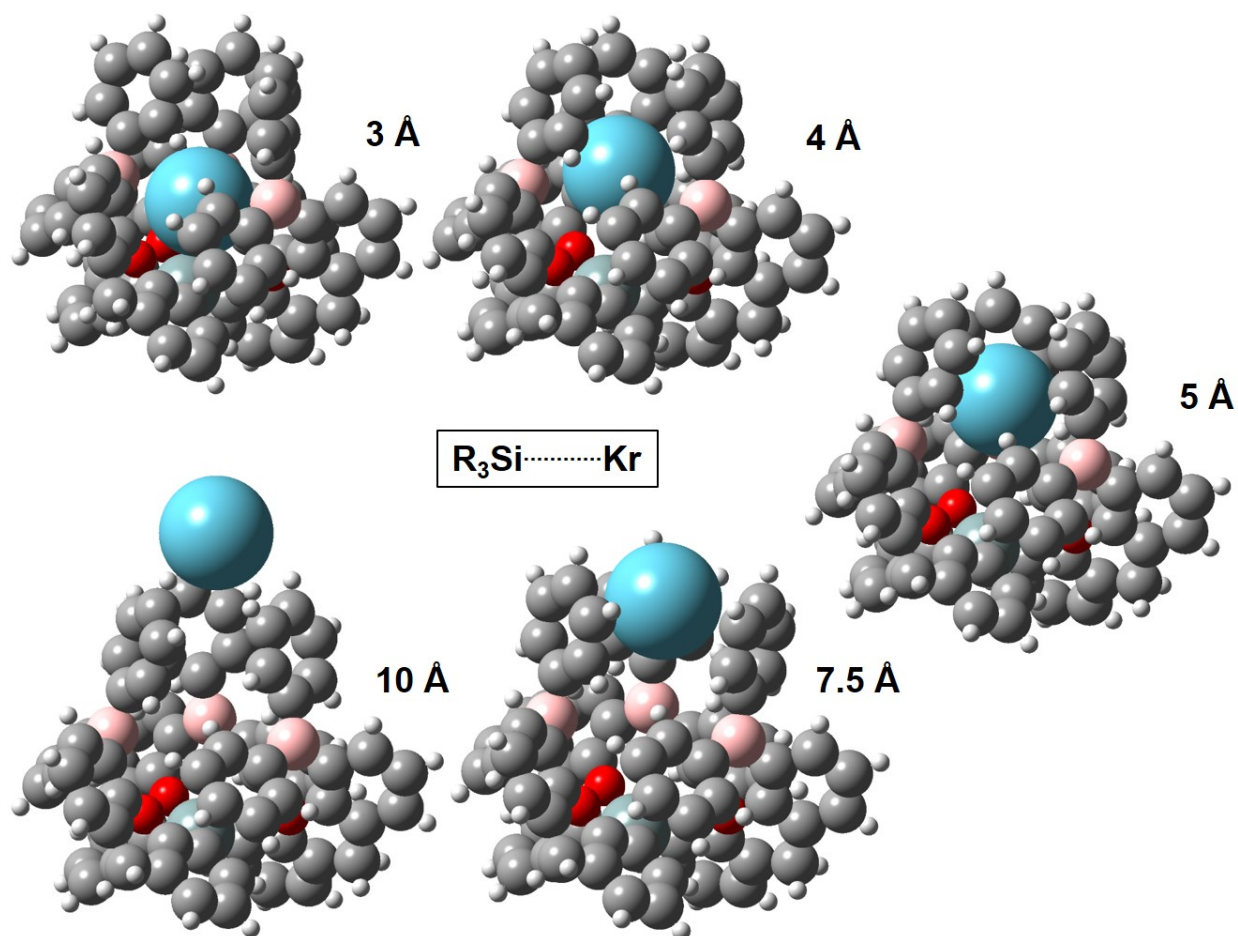
Figure S6. Si⋯Kr distance constrained relaxed gas-phase geometries of [(5-Ph$_2$B-*xan*-4-)$_3$Si·Kr]$^+$ (potential energy scan of **2g**): Van der Waals representation. VdW-radii used as implemented in GaussView3. Color code: Si (light gray), O (red), B (yellow), Kr (deep blue).
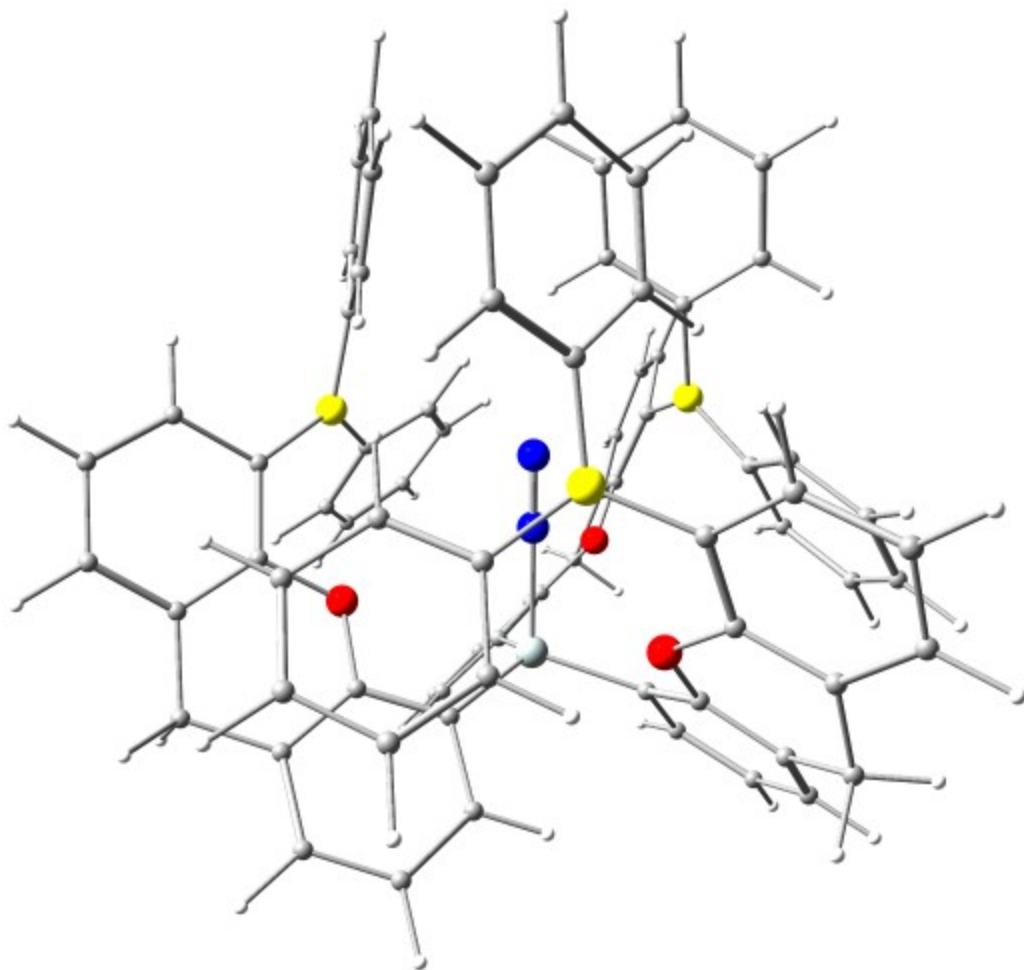
Figure S7. Relaxed gas-phase geometry of [(5-Ph$_2$B-*xan*-4-)$_3$Si·N$_2$]$^+$. N$_2$-adduct formation is energetically favored by -74.7 kJ mol^{-1} (ΔE) and thermodynamically by -53.5 kJ mol^{-1} (ΔG). Both values are corrected for BSSE (7.4 kJ mol^{-1}).
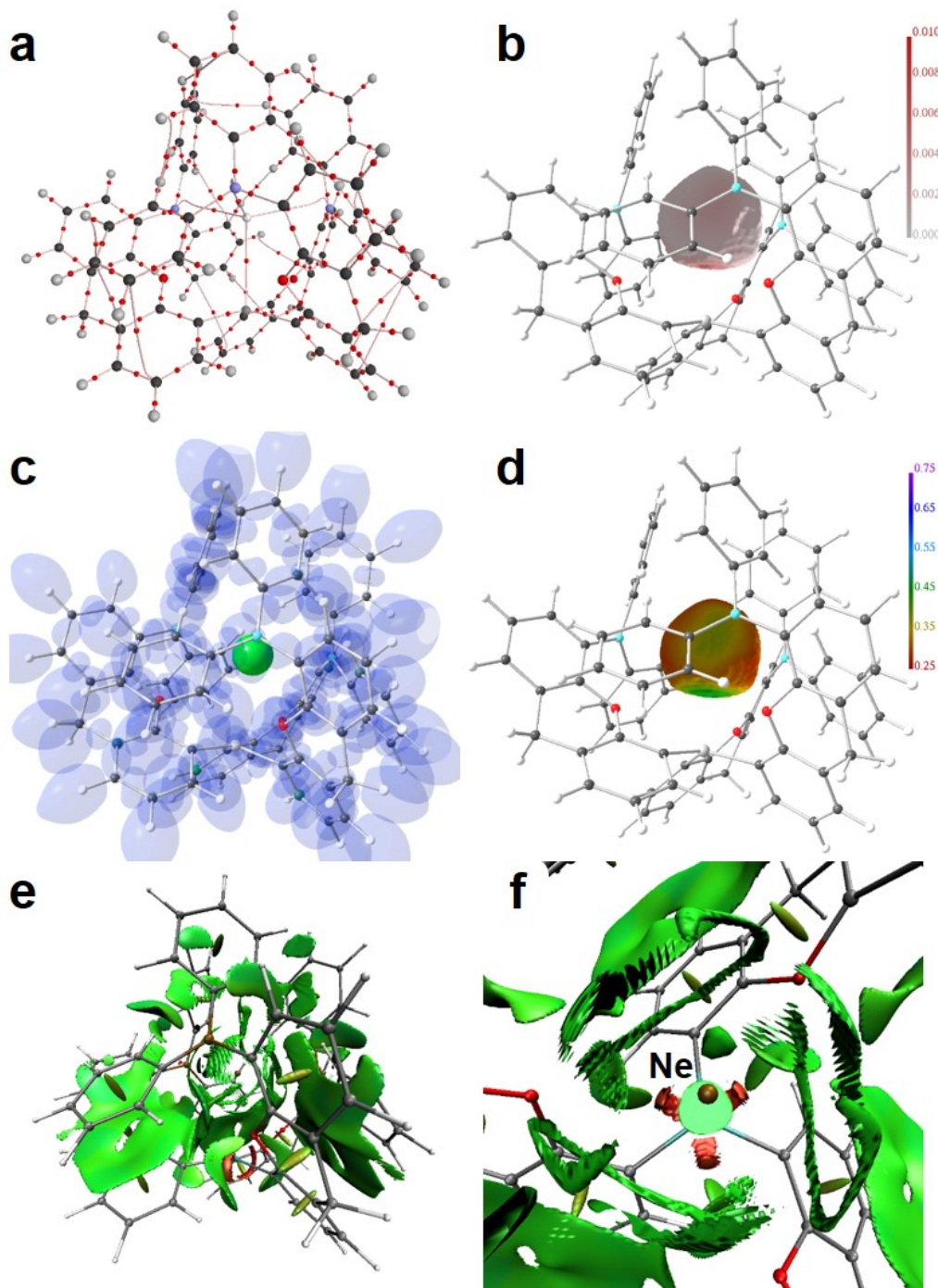
Figure S8. RSBI analysis of [(5-Ph$_2$B-*xan*-4-)$_3$Si·Ne]$^+$ (**2e**) (a) AIM bond paths motif, (b) ED distribution (in a.u.) mapped on the AIM atomic basin of Ne, (c) ELI-D localization domain representation at an *iso*-value of 1.35, (d) ELI-D distribution mapped on the Ne ELI-D bonding basin, (e) NCI *iso*-surface at s(**r**) = 0.5, (f) Magnification of the binding site; top view.
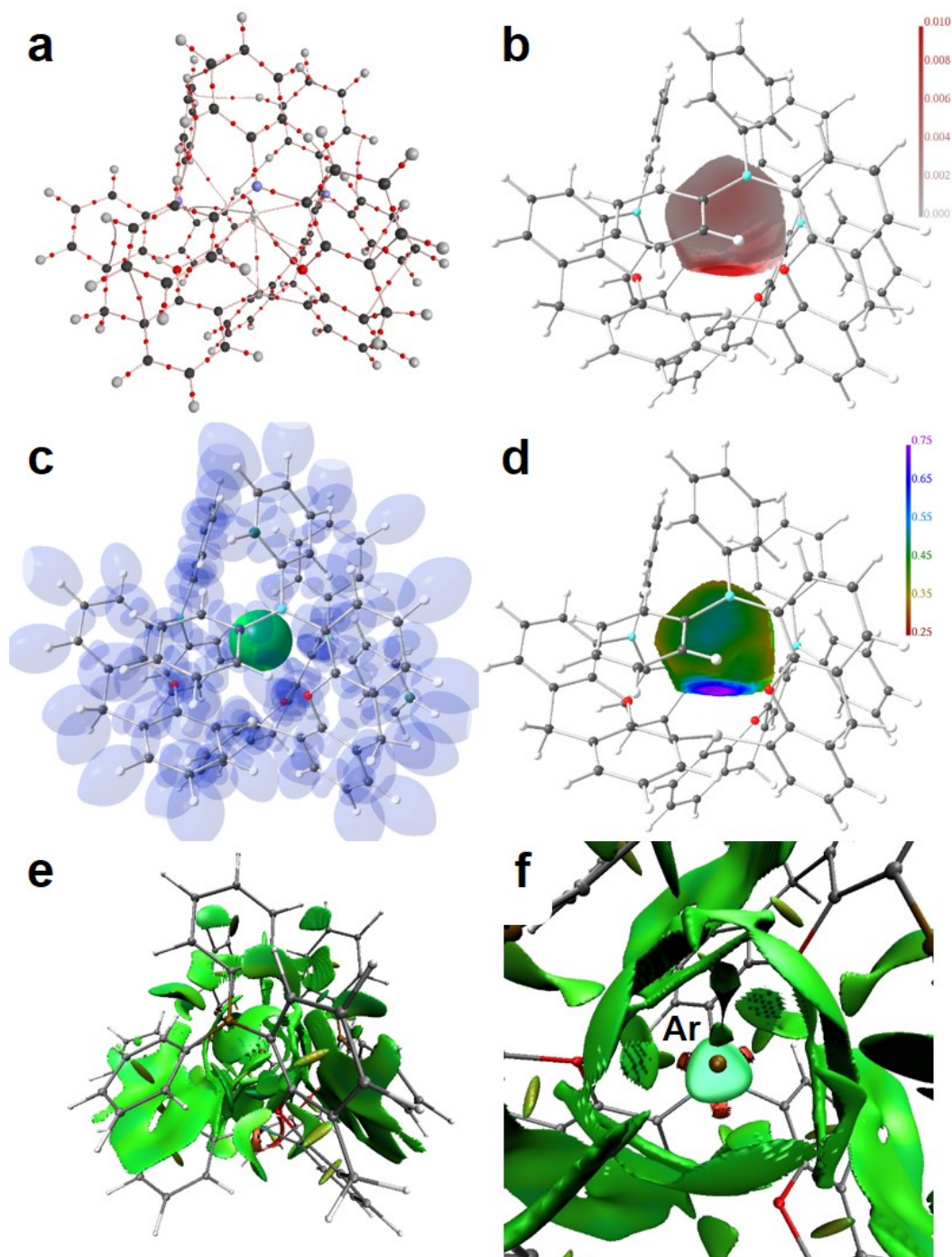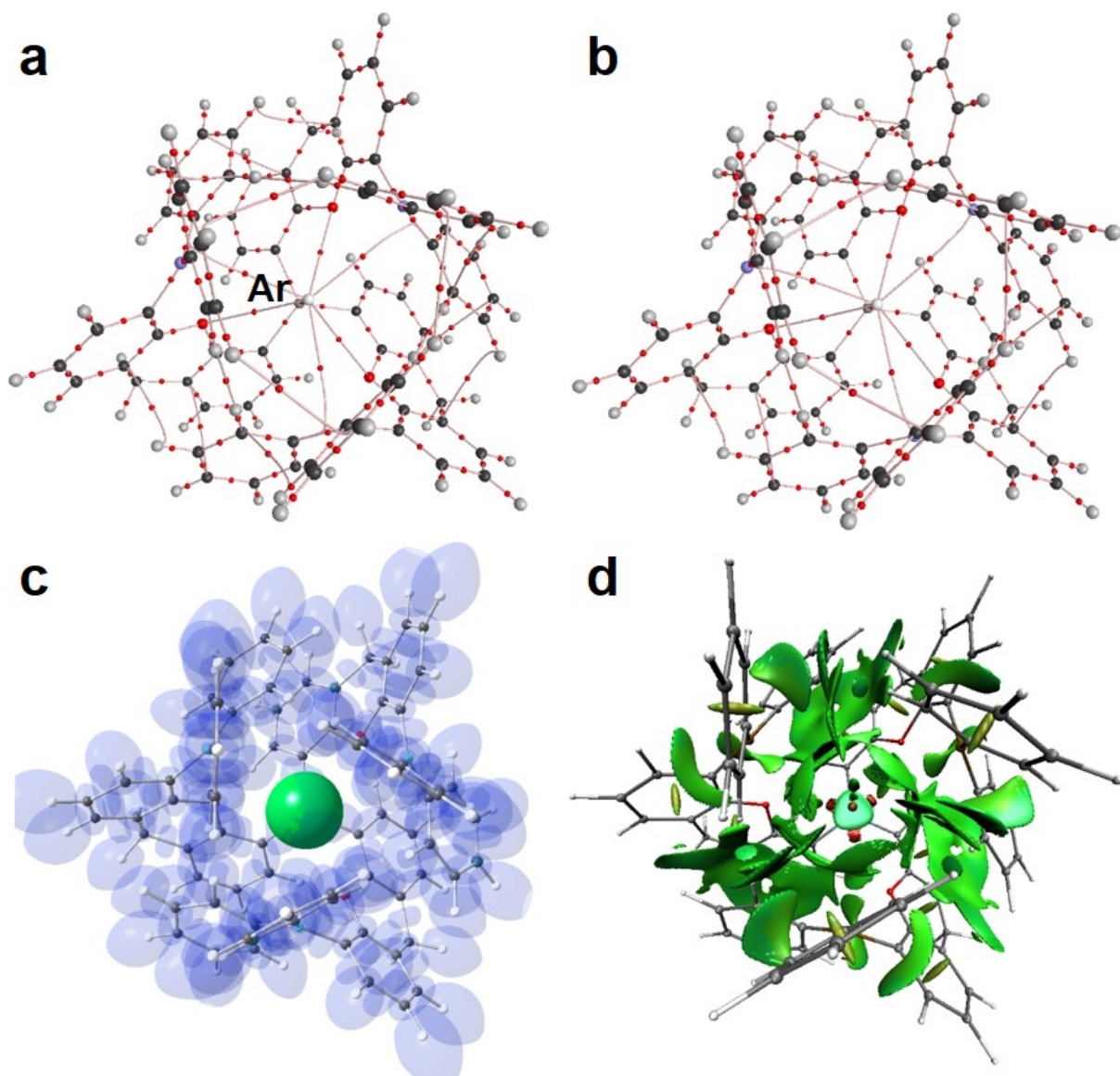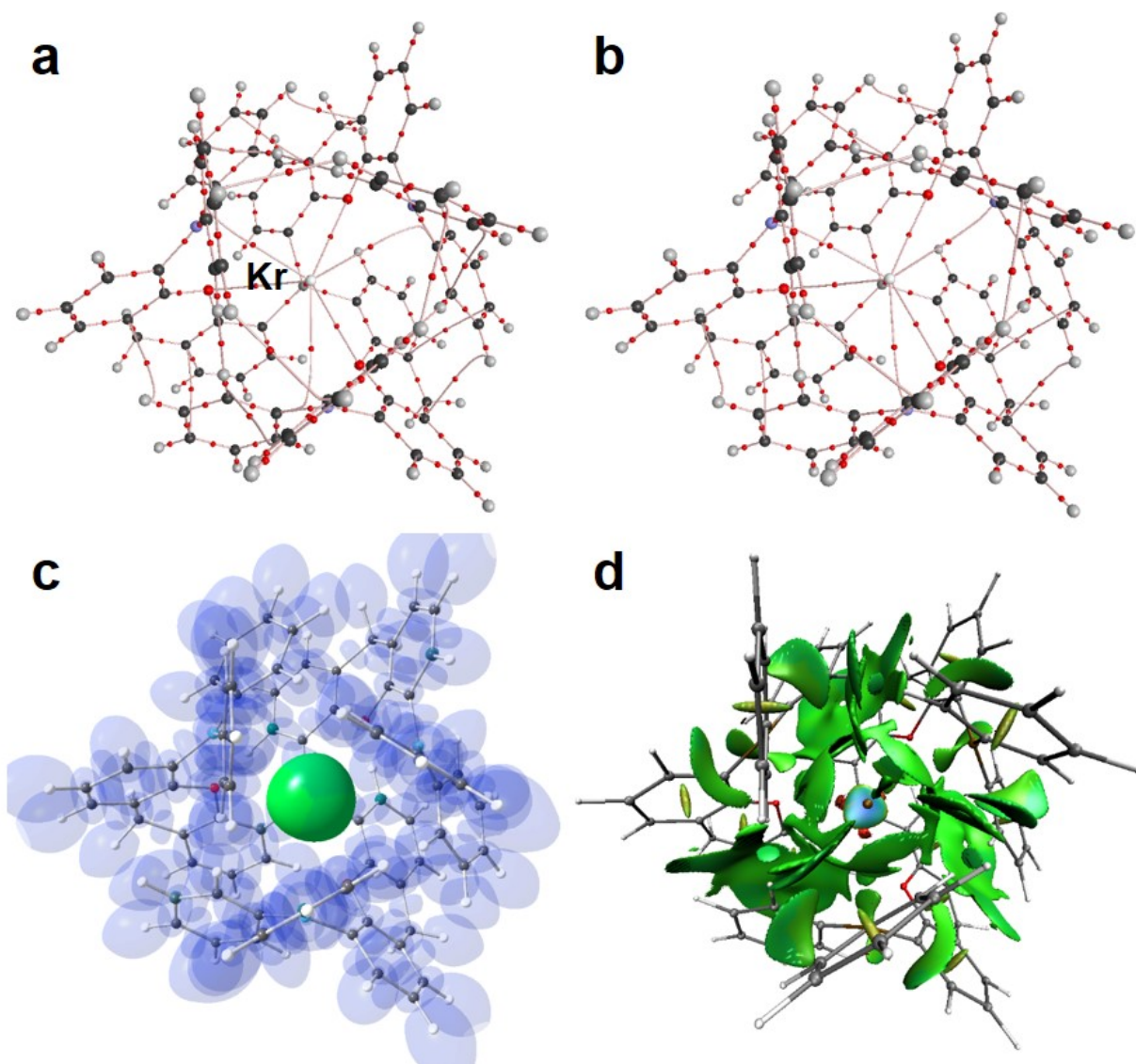
Figure S9. RSBI analysis of [(5-Ph$_2$B-*xan*-4-)$_3$Si·Ar]$^+$ (**2f**): (a) AIM bond paths motif, (b) ED distribution (in a.u.) mapped on the AIM atomic basin of Ar, (c) ELI-D localization domain representation at an *iso*-value of 1.35, (d) ELI-D distribution mapped on the Ar ELI-D bonding basin, (e) NCI *iso*-surface at s(**r**) = 0.5, (f) Magnification of the binding site; top view.
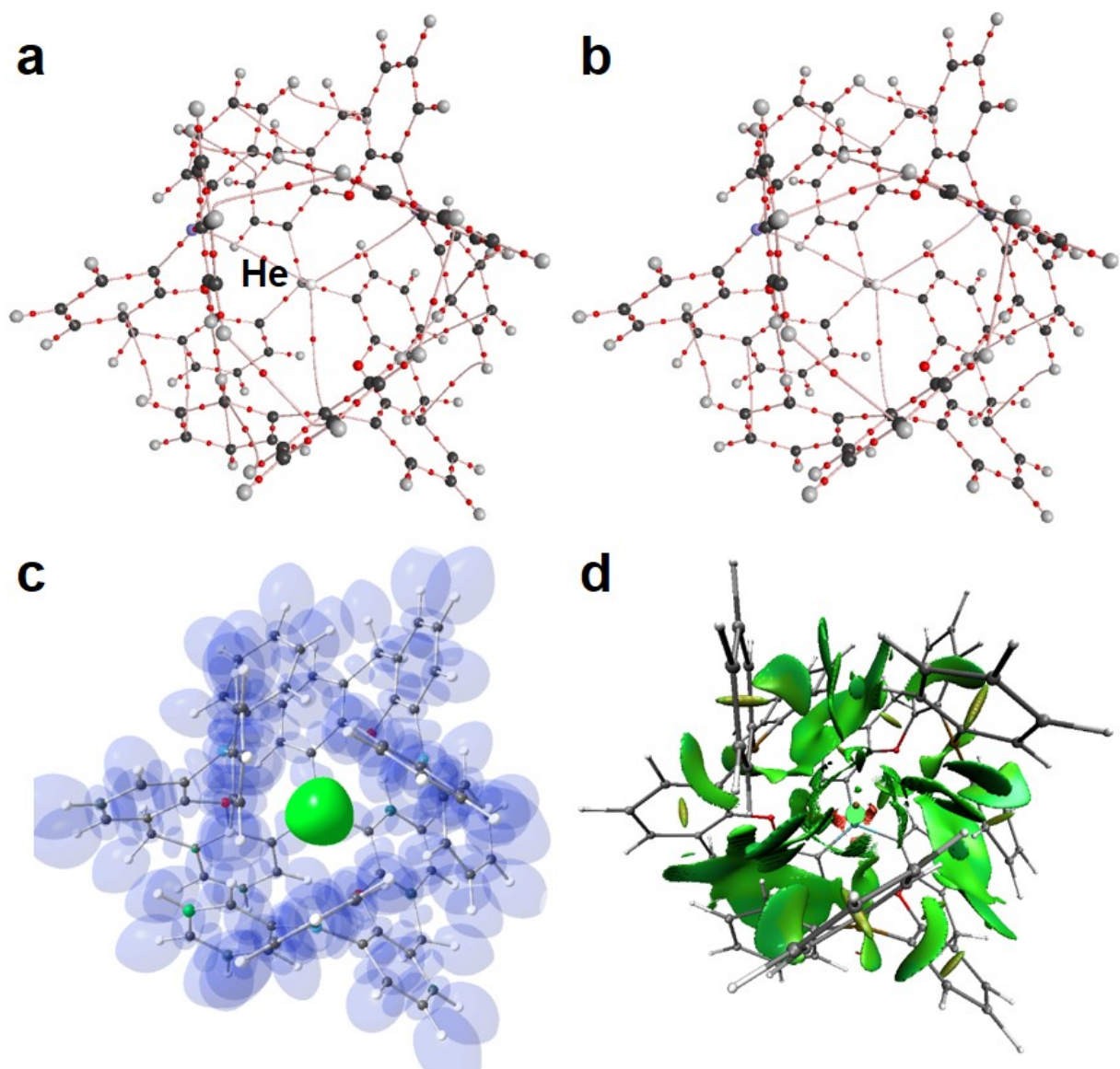
Figure S10. RSBI analysis of [(5-Ph$_2$B-*xan*-4-)$_3$Si·He]$^+$ (**2d**): Top view. (a) AIM bond paths motif, (b) Virial field paths motif, (c) ELI-D localization domain representation at an *iso*-value of 1.35, (d) NCI *iso*-surface at s(**r**) = 0.5.
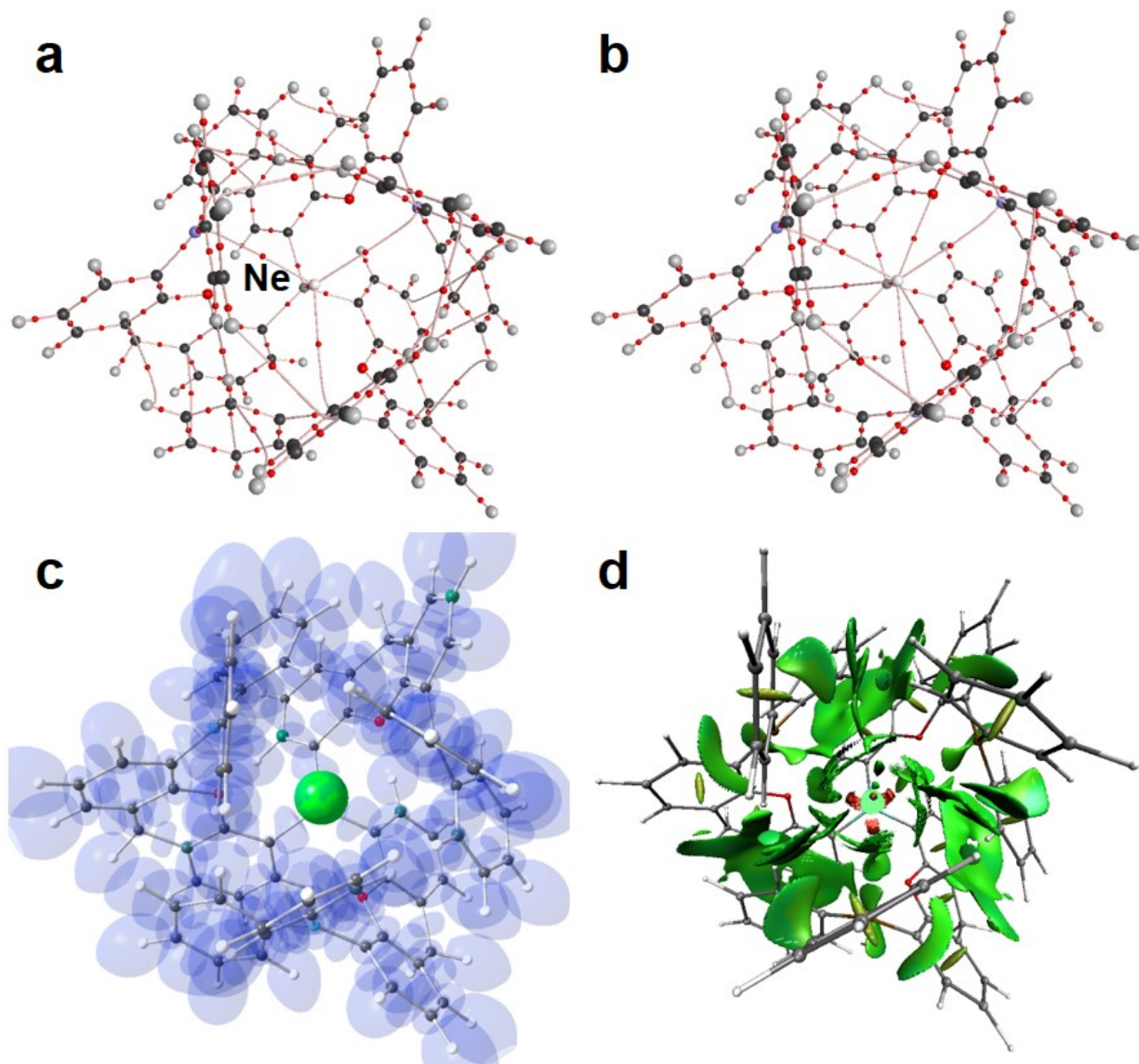
Figure S11. RSBI analysis of [(5-Ph$_2$B-*xan*-4-)$_3$Si·Ne]$^+$ (**2e**): Top view. (a) AIM bond paths motif, (b) Virial field paths motif, (c) ELI-D localization domain representation at an *iso*-value of 1.35, (d) NCI *iso*-surface at s(**r**) = 0.5.

Figure S12. RSBI analysis of [(5-Ph$_2$B-*xan*-4-)$_3$Si·Ar]$^+$ (**2f**): Top view. (a) AIM bond paths motif, (b) Virial field paths motif, (c) ELI-D localization domain representation at an *iso*-value of 1.35, (d) NCI *iso*-surface at s(**r**) = 0.5.

Figure S13. RSBI analysis of [(5-Ph$_2$B-*xan*-4-)$_3$Si·Kr]$^+$ (**2g**): Top view. (a) AIM bond paths motif, (b) Virial field paths motif, (c) ELI-D localization domain representation at an *iso*-value of 1.35, (d) NCI *iso*-surface at s(**r**) = 0.5.
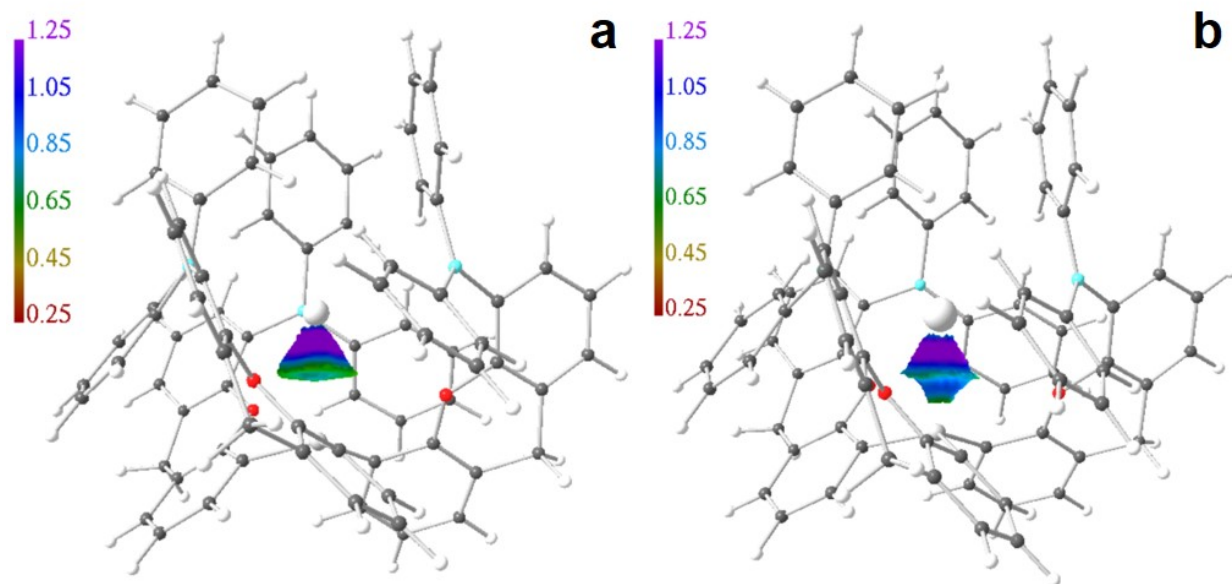
Figure S14. Disynaptic (bonding) ELI-D Ng–Si basins for [(5-Ph$_2$B-*xan*-4-)$_3$Si·Ar]$^+$ (**2f**) and [(5-Ph$_2$B-*xan*-4-)$_3$Si·Kr]$^+$ (**2g**).